THE JOURNAL OF PHYSICAL CHEMISTRY B

Article

pubs.acs.org/JPCB

Putative Hydrogen Bond to Tyrosine M208 in Photosynthetic Reaction Centers from *Rhodobacter capsulatus* Significantly Slows Primary Charge Separation

Miguel Saggu,[†,§] Brett Carter,[†] Xiaoxue Zhou,[†] Kaitlyn Faries,[‡] Lynette Cegelski,[†] Dewey Holten,[‡] Steven G. Boxer,[†] and Christine Kirmaier*[,‡]

[†]Department of Chemistry, Stanford University, Stanford, California 94305-5012, United States

[‡]Department of Chemistry, Washington University, St. Louis, Missouri 63130-4899, United States

Supporting Information

ABSTRACT: Slow, ~50 ps, P* → $P^+H_A^-$ electron transfer is observed in *Rhodobacter capsulatus* reaction centers (RCs) bearing the native Tyr residue at M208 and the single amino acid change of isoleucine at M204 to glutamic acid. The P* decay kinetics are unusually homogeneous (single exponential) at room temperature. Comparative solid-state NMR of [4′-^{13}C]Tyr labeled wild-type and M204E RCs show that the chemical shift of Tyr M208 is significantly altered in the M204E mutant and in a manner consistent with formation of a hydrogen bond to the Tyr M208 hydroxyl group. Models based on RC crystal structure coordinates indicate that if such a hydrogen bond is formed between the Glu at M204 and the M208 Tyr hydroxyl group, the −OH would be oriented in a fashion expected (based on the calculations by Alden et al., *J. Phys. Chem.* **1996**, *100*, 16761−16770) to destabilize $P^+B_A^-$ in free energy. Alteration of the environment of Tyr M208 and B_A by Glu M204 via this putative hydrogen bond has a powerful influence on primary charge separation.

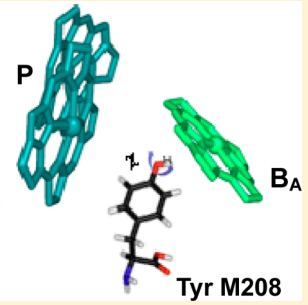

INTRODUCTION

Perhaps no amino acid in the bacterial photosynthetic reaction center (RC; Figure 1A)[1−3] has been scrutinized more than the tyrosine situated near the dimeric bacteriochlorophyll (BChl) primary electron donor (P) and the monomeric BChl initial electron acceptor (B_A) on the A-side of the RC. This residue is Tyr M208 in *Blastochloris viridis* and *Rhodobacter capsulatus* and Tyr M210 in *Rhodobacter sphaeroides*. Both theoretical work[4−10] and experiments on mutants[11−44] have led to consensus that this conserved residue is a significant contributor to extremely rapid and efficient initial A-side charge separation. Interestingly, there are no potential hydrogen bond partners available to Tyr M208, which is unique among the roughly 28 (depending on species) tyrosines in the RC. Consistent with this, a unique chemical shift is observed in the ^{13}C NMR spectrum for the 4′-C-carbon (the carbon bonded to the −OH) of this unique Tyr.[45,46] Replacing the Phe residue at the C_2-symmetry related site, L181 near B_B, with a Tyr often has been a design element in eliciting electron transfer (ET) from P* to the bacteriopheophytin (BPh) on the B-side (H_B).[47−61] However, P* → $P^+H_B^-$ conversion is at best more than an order of magnitude slower than initial charge separation on the A-side. The RC ET dynamics have long been modeled in the context of the state free-energy relationships shown in Figure 1B. Here $P^+B_A^-$ lies between P* and $P^+H_A^-$ in free energy with the analogous B-side states placed somewhat higher and in particular with $P^+B_B^-$ above P*. These orderings are consistent with a general picture of rapid (1−3 ps) steps of ET from P* to B_A and then to H_A with details and mechanisms under continuing study.[62−67] Slower, noncompetitive, ET to H_B is presumably superexchange mediated by B_B. Electrostatic calculations by Alden et al. suggested that a specific orientation of the hydroxyl group of Tyr M208 having the −OH pointing toward B_A stabilizes $P^+B_A^-$.[8] In addition, this was found to be the strongly preferred orientation over a second, where the −OH is rotated ~180° about the C−O bond and which, in comparison, destabilizes $P^+B_A^-$. The calculations predicted that the stabilization of $P^+B_A^-$ induced by the −OH of Tyr M208 in the preferred orientation is a significant ~200 meV. Note that a possible corollary of this sensitivity is the expectation that the initial ET reactions may be inhomogeneous, depending on the timescale of the −OH dipole motion, and in fact nonsingle exponential kinetics are commonly observed for these reactions.

The preferred orientation of the −OH dipole is not known experimentally given the current resolution of even the best X-ray structures. Therefore, we consider the simulations of Alden et al. as providing a working hypothesis for contemplating further protein engineering. An expanded view of the region around Tyr M208 and B_A is illustrated in Figure 2 in a homology model of the *Rb. capsulatus* RC.[68] Residue M204 is the closest amino acid to the Tyr M208. Therefore, we replaced isoleucine M204 with glutamic acid and glutamine to introduce a potential hydrogen bond acceptor for the −OH of tyrosine M208. As reported previously, to our surprise, the M204Q

Received: April 7, 2014
Revised: May 15, 2014
Published: June 6, 2014

   dx.doi.org/10.1021/jp503422c | *J. Phys. Chem. B* 2014, 118, 6721−6732

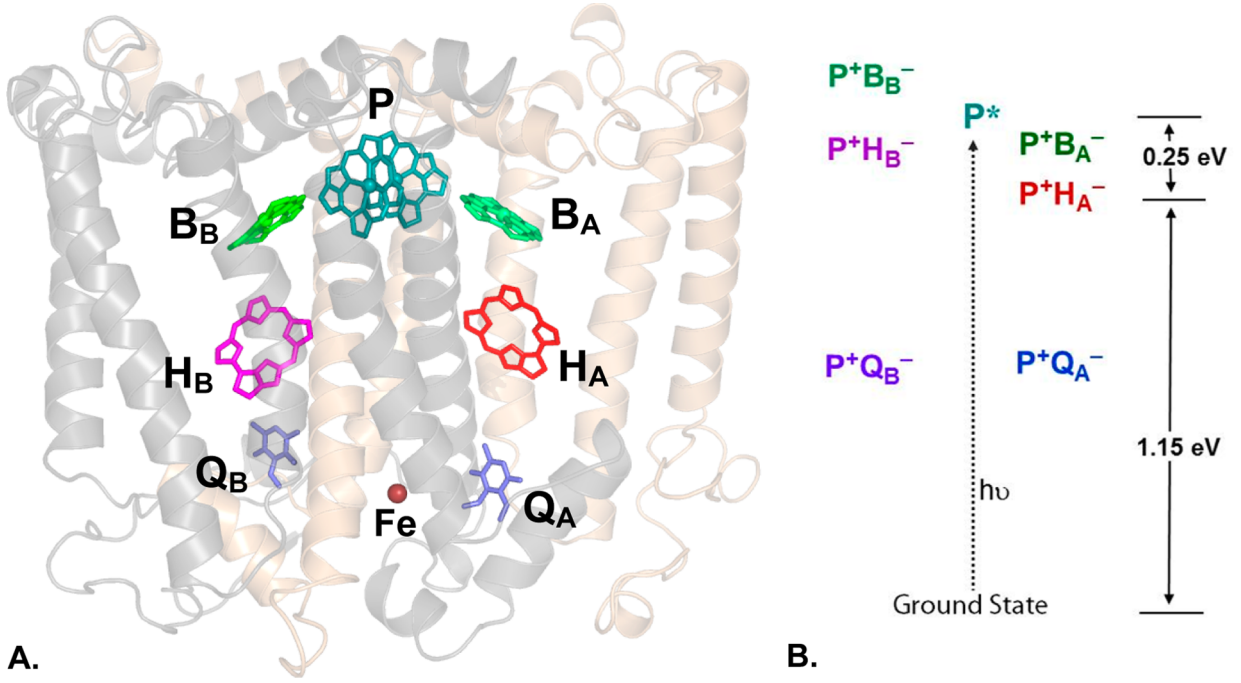

Figure 1. (A) Reaction center pigment protein complex from the *Rb. sphaeroides* X-ray crystal structure (Protein Data Bank: 2j8c). (B) Model free-energy diagram for WT RCs.

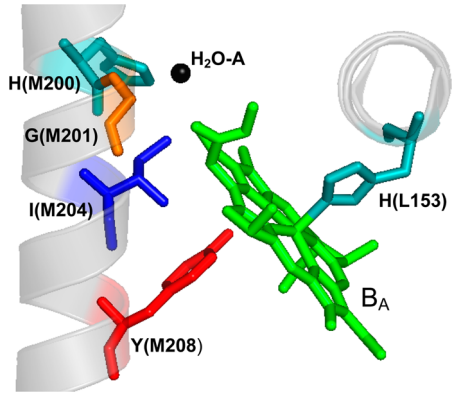

Figure 2. View of the environment of B_A as determined in the wild-type *Rb. sphaeroides* RC crystal structure (Protein Data Bank: 2j8c). Note that the numerical values and amino acids of the L and M polypeptides correspond to those of RCs from *Rb. capsulatus*. His M200 (M202 in *Rb. sphaeroides*) is a ligand to the M-BChl macrocycle of P (not shown).

mutation leads to complete loss of B_A.[55] Ultrafast measurements on M204Q RCs gave the expected results of substantial deactivation of P* to the ground state, no A-side ET, and a small yield of B-side charge separation, P* → $P^+H_B^-$, that was increased upon changing Phe at L181 to a Tyr.[55] We report here that substitution of M204 with glutamic acid leads to altogether different results. Modeling of Glu at M204 using Pymol suggests that if a hydrogen bond to the Tyr M208 hydroxyl group is formed, the hydroxyl group would be held in an orientation that disfavors P* → $P^+H_A^-$ ET, noting, though, that the energetic consequences of a hydrogen-bonded tyrosine −OH in this orientation may be different from the non-hydrogen-bonded case of the simulations (in ref 8). With the use of uniformly [4′-^{13}C]-labeled Tyr, the ^{13}C NMR spectrum reveals that Tyr M208 in M204E no longer has the unique chemical shift associated with Tyr M208 not being hydrogen bonded, as in wild-type, consistent with the introduction of a hydrogen bond. Ultrafast measurements of M204E RCs reveal that reduction of H_A is about a factor of 10 slower than in wild-type and that the room temperature P* decay kinetics are unusually homogeneous.

EXPERIMENTAL SECTION

Mutagenesis and RC Isolation. The native isoleucine residue at M204 in the *Rb. capsulatus* RC was changed to a glutamic acid by site-directed mutagenesis, as described previously,[52] using the QuikChange mutagenesis kit (Stratagene). RC isolation and purification followed published procedures[55,61] utilizing 0.1% Deriphat 160-C for protein solubilization for transient absorption or 0.1% *N,N*-dimethyldodecylamine *N*-oxide (LDAO) for NMR and mass spectrometry. Measurements were conducted on RCs in 10 mM Tris (pH 7.8) and 0.1% Deriphat 160-C, unless noted otherwise. Protein purity was examined using SDS−PAGE with a 4−15% gradient gel.[69]

RC Pigment Analysis. Wild-type and M204E RCs were extracted using acetone/MeOH (7:2 v/v) and the BChl:BPh pigment ratio determined spectroscopically, as according to van der Rest et al.[70] The pigment content was also assayed by HPLC because of the unusual results reported below. For this, the acetone/MeOH extract was dried under a stream of nitrogen and dissolved in acetonitrile/ethyl acetate/MeOH/water (24:20:47:9 v/v). After filtration through a 0.22 μm filter, the pigments were analyzed using an Agilent Infinity 1260 HPLC setup equipped with an analytical C18 column (Spherisorb C18, 4.6 × 250 mm, 5 μm) and a multiple wavelength detector (1260 MWD VL). Pigments were detected at 770 nm using isochratic elution with acetonitrile/ethyl acetate/MeOH/water (24:20:47:9 v/v) at a flow rate of 1 mL/min.

Preparation of ^{13}C-labeled RC. *Rb. capsulatus* cells were grown in a bioreactor (New Brunswick Scientific, BioFlo3000,

dx.doi.org/10.1021/jp503422c | J. Phys. Chem. B 2014, 118, 6721−6732

5 L) under controlled pH and oxygen levels in the dark to maximize RC yield. To incorporate labeled [4′-^{13}C]Tyr, a modified ^{Super}RCVPY media[71] was used that substituted peptone and yeast extract with a defined amino acid composition, as according to Raap et al.[72] A small amount of antifoam 204 (Sigma-Aldrich) was added before inoculation. The optimal growth conditions were as follows: the culture pH was maintained at 6.8 with a titration solution containing 4 M DL-malic acid with an agitation rate of 500 rpm at a temperature of 34 °C. The atmosphere was controlled using a nitrogen/air mixture (95:5), and the dissolved oxygen level was monitored using an oxyprobe. The oxyprobe was calibrated using a two-point calibration with 100% air and 100% nitrogen as reference values.

Mass Spectrometry. The incorporation of labeled [4′-^{13}C]Tyr (Cambridge Isotopes) was quantitated by performing LC−MS/MS on digested wild-type RCs. Samples were subjected to in-solution digestion using urea and ProteaseMAX (Promega) and a combination of trypsin/α-chymotrypsin to cut out the peptide of interest that contains tyrosine M208 (fragment M200-M208). Briefly, 50 μg protein was precipitated with 4 volumes of −20 °C acetone and incubated at −80 °C for 20 min. After centrifugation, the white pellet (blue-green pellet in case of M204E) was rinsed with 300 μL acetone and allowed to air-dry for 5 min. Then, 15 μL of 8 M urea and 20 μL of 0.2% ProteaseMAX were added, and the solution was vortexed for 5 min to solubilize the pellet. The mixture was placed in a shaker at 25 °C and 140 rpm for 1 h. After solubilization, the sample was reduced with dithiothreitol, alkylated with iodoacetamide, and digested using trypsin/α-chymotrypsin (1.8 μg in total) and ProteaseMAX at 37 °C for 3 h. The digestion was stopped by addition of 2 μL 25% trifluoroacetic acid. To remove particles, the sample was centrifuged for 10 min at 16000 rpm. Peptides were purified using a stage-tip C18 column. In the first step, the column was washed with acetonitrile and in the second step with water/0.1% formic acid. The sample was loaded and washed with water containing 0.1% formic acid. Peptides were eluted using acetonitrile/water/formic acid (60:40:0.1). Mass spectra were obtained on a Thermo LTQ-Orbitrap Velos mass spectrometer equipped with a nanoHPLC (C18, 100 μm i.d., 15 cm length, 3 μm particle size). The peptides were eluted using a gradient running from water (containing 0.1% formic acid) to acetonitrile over the course of 60 min (3−40% for 40 min, 40−65% for 10 min, 65−95% for 5 min, and 95−3% for 5 min). The mass accuracy of the Orbitrap and of the ion trap are below 2 ppm and around 250 ppm, respectively.

Solid-State NMR Spectroscopy. Labeled RCs (25 mg) were reconstituted into lipids and lyophilized to ensure a homogeneous environment and a dry sample following described procedures.[73] L-α-Phosphatidylcholine (Egg PC) was dissolved in 10 mM Tris pH 8 buffer containing 0.58% n-dodecyl-ß-D-maltoside. Twenty-five milligrams RC was added and the total volume was 5 mL (1:100 mol % of protein/lipid). Biobeads-SM2 were washed vigorously with MeOH, water, and finally 10 mM Tris, pH 8. The beads were added (~110 mg, 5-fold w/w excess over detergent), and the solution was stirred overnight in the dark at 4 °C to remove detergent. The next day, another 110 mg of biobeads-SM2 were added and the solution was stirred for another 3 h. The beads were removed by filtration, trehalose was added as cryoprotectant to a final concentration of 25 mM, and the solution was stirred at 4 °C for 15 min. The sample was slowly frozen at −20 °C, and then transferred to −80 °C and finally frozen in liquid nitrogen. The frozen sample was attached to a lyophilizer and dried for 3 days. The resulting powder was packed into a 5 mm zirconia rotor. Solid-state NMR experiments were performed with an 89 mm wide-bore Varian/Agilent magnet at 11.7 T (125.49 MHz for ^{13}C), Varian console, and a home-built four-frequency transmission-line probe with a 13.6 mm long, 6 mm inner-diameter sample coil and a Revolution NMR MAS Vespel stator. Samples were spun at 8000 ± 2 Hz, using a Varian MAS control unit and cooled with −30 °C nitrogen gas. The proton-carbon matched cross-polarization transfer was performed at 83 kHz, and the recycle delay was 2 s. The chemical shift scale was referenced to external adamantane.

Ultrafast Measurements. Ultrafast transient absorption (TA) measurements were carried out on an apparatus that utilizes ~120 fs excitation and white-light probe flashes delivered at a repetition rate of 10 Hz. In order to ensure that fresh sample was interrogated on each excitation flash, RCs were flowed from a small reservoir through a 2 mm path length cell used for the pump/probe interrogation. The RCs were kept at ~10 °C by use of an ice bath to cool the reservoir. Further details of the instrumentation and can be found elsewhere.[48] The TA data were analyzed using Origin (Microcal) and Surface Explore (Ultrafast Systems). Kinetic simulations were performed using the freely available program KinSim.[74]

Spectrochemical Redox Measurements. The P/P^+ midpoint potential was obtained using a SEC-C thin layer quartz glass cell (BASi EF-1358), platinum counter electrode (BASi EF-1356), a Ag/AgCl double junction reference electrode (BASi MF-2079, MF-2030) and ferricyanide as the oxidizing species. The reference electrode was calibrated using standard solutions.[75] The titration starting conditions were 750 μL of ~20 μM RCs and 4 mM potassium ferrocyanide (to ensure initial fully reduced RCs) in 10 mM Tris, pH 7.6, and 0.1% Deriphat. Small increments (starting with ~0.25 μL and gradually increasing to ~10 μL as the titration proceeded) of stock 1 M potassium ferricyanide in 10 mM Tris, pH 7.6, and 0.1% Deriphat were added directly to the sample in the cell and mixed by gentle pipetting several times over the course of 10 min. The absorbance at ~865 nm was then measured (Shimadzu UV-1800) and the potential (voltage) recorded. The titrations were stopped when addition of ferricyanide no longer altered the measured potential or when the absorption of the ferricyanide began to interfere with reading the RC absorbance (generally when approaching ~50 μL total ferricyanide stock added).

RESULTS

Cell Growth. In order to work with the minimal amount of [4′-^{13}C]Tyr-labeled media, cell growth of *Rb. capsulatus* was optimized in a bioreactor under controlled conditions. Previous studies on *Rp. viridis* have shown that RC gene expression can be enhanced by growing cells under microaerophilic conditions in the dark.[76,77] A series of experiments determined the optimum dissolved oxygen level for maximum protein expression. Holding the dissolved oxygen level constant around 2% for the last few hours before harvesting cells around OD_{660} ≈ 5 gave good protein expression (Figure S1 of the Supporting Information), about a 3-fold increase in protein yield (>60 mg purified protein per 4 L growth medium).

Mass Spectrometry. To determine the amount of [4′-^{13}C]Tyr at position M208 incorporated under our conditions, LC−MS/MS was performed on trypsin/α-chymo-

dx.doi.org/10.1021/jp503422c | J. Phys. Chem. B 2014, 118, 6721−6732

trypsin-digested RC. To our knowledge, mass spectrometry of fragments of bacterial RC proteins has not been previously reported and a more detailed analysis can be found elsewhere.[78] One problem is the hydrophobicity of large stretches the RC, which makes proteolytic digestion difficult in the absence of detergent. In previous work on RCs, detergent was removed by precipitation, and the pellet was treated with 8 M urea.[78] Digestion with trypsin or α-chymotrypsin yielded only low sequence coverage for H, L, and M subunits (54% H, 14% M, and 10% L with trypsin; 15% H, 15% M, and 18% L with α-chymotrypsin). In the present study, the pellet was solubilized after detergent removal using ProteaseMAX, which solubilizes during proteolytic digestion, resulting in much higher sequence coverage, in particular for the hydrophobic L and M subunits (60% H, 54% M, and 41% L).

For our purpose, a combination of trypsin/α-chymotrypsin was used because this treatment releases a peptide corresponding to residues M200-M208 (sequence HGLSIAALY). Both labeled and unlabeled wild-type RCs were digested and are compared in Figure S2 of the Supporting Information. The peptide HGLSIAALY has a m/z value of 473.76 for the doubly charged ion. Comparison with the [4′-^{13}C]Tyr labeled wild-type shows that the whole isotope pattern is shifted by m/z = 0.5, indicating >99% incorporation of label (the mass accuracy of Orbitrap mass analyzers is <2 ppm). These results are consistent with previous work on *Rb. sphaeroides* RCs, where a high concentration of [4′-^{13}C]Tyr in the media was found to be necessary to compete with tyrosine biosynthesis and ensure quantitative incorporation of label into the RC.[45,72] In the previous studies, total hydrolysis of the RC was performed to quantify total [4′-^{13}C]Tyr incorporation,[72] whereas our approach provides a direct method to quantify site-specific labels using LC−MS/MS.

Solid-State NMR Spectroscopy. NMR spectroscopy is a useful technique to monitor the protonation and hydrogen bond status of the tyrosine hydroxyl group using the chemical shift of [4′-^{13}C]Tyr, as shown in numerous studies.[45,79,80] Figure 3 shows the ^{13}C CPMAS NMR spectrum of [4′-^{13}C]Tyr-labeled wild-type and M204E RCs obtained at 230 K. The *Rb. capsulatus* RC contains 31 tyrosines, and this accounts for the major and unresolved [4′-^{13}C]Tyr peak between 154 and 158 ppm, typical for protonated and hydrogen-bonded Tyr. In wild-type, a small, well-resolved peak is observed upfield from this at around 153 ppm. This spectrum is similar to that found for [4′-^{13}C]Tyr-labeled wild-type RCs from *Rb. sphaeroides*, where this peak could be attributed to Tyr M210 (equivalent to M208 in *Rb. capsulatus*) using site-directed mutagenesis. Notably, Tyr M208/M210 is the only tyrosine that is not hydrogen bonded and the upfield shift is typical of this effect.[45,46,81] The X-ray structure of *Rb. sphaeroides* RCs confirms that there is no hydrogen bond acceptor in close proximity to the Tyr M210 hydroxyl group.[1] Note that there may also be some contribution to this shift from the ring current of B_A.

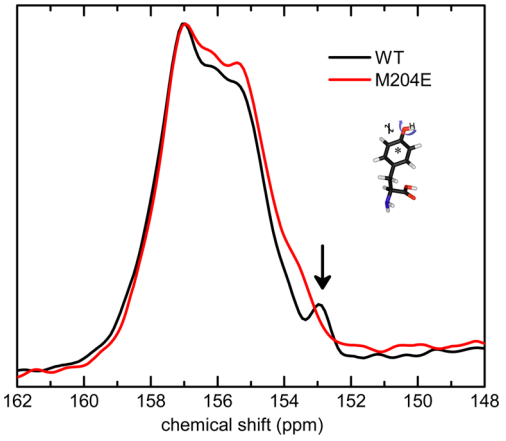

Figure 3. ^{13}C CPMAS solid-state NMR of [4′-^{13}C]Tyr labeled RCs at T = 230 K. The unique resolved peak at 153 ppm (↓) in WT (wild-type) RCs is assigned to the 4′-^{13}C carbon (*) of Tyr M208. It is shifted back into the poorly resolved broad band corresponding to all the other hydrogen bonded tyrosines in the M204E mutant. Each spectrum is the result of 32768 scans.

The ^{13}C NMR spectrum of M204E with [4′-^{13}C]Tyr (Figure 3) clearly shows a significant change compared with wild-type. The unique upfield-shifted peak at 153 ppm is absent in M204E, apparently shifted back into the unresolved peak containing all the other hydrogen-bonded tyrosine residues in the RC. This result suggests that the introduced glutamic acid at M204 creates a hydrogen bond to the hydroxyl group of Tyr M208 as designed.

Absorption Spectrum and Pigment Analysis. As noted above, the M204Q mutant assembles without B_A, as reflected in the absorption spectrum and determined by analysis of the pigment content.[55] As shown in Figure 4, the 77 K absorption

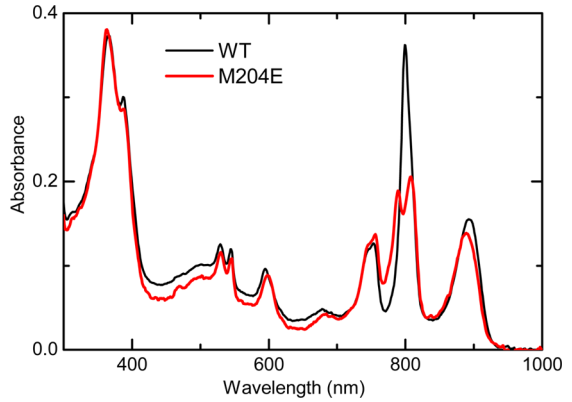

Figure 4. Low-temperature UV/vis/NIR spectra obtained at 77 K. The spectra are normalized at 366 nm for comparison.

spectrum of M204E RCs has two bands near 800 nm that are assigned to B_A and B_B. In the wild-type spectrum in Figure 4, the Q_Y bands of B_A and B_B are not resolved; however, different detergent or buffer conditions and some mutations also lead to partial resolution of these bands. The RC pigment contents of wild-type and M204E RCs were assayed via the standard spectroscopic method.[70] Following extraction of RCs with acetone:MeOH (7:2, v/v), the solution is filtered before acquiring the UV/vis/NIR spectrum in order to minimize the contribution of protein light-scattering. BChl/BPh ratios of 1.4 for M204E and 1.9 for wild-type were determined, indicating extraction of only 3 BChls from the M204E RC. The same results were obtained if instead of filtering the extraction solution it was centrifuged for 1 min in a benchtop unit. Confirming incomplete extraction of pigment from M204E RCs, the pelleted residue from M204E is blue-green, whereas for wild-type it is pale yellow (Figure S3 of the Supporting Information). Attempts to extract a (presumed) BChl pigment

dx.doi.org/10.1021/jp503422c | J. Phys. Chem. B 2014, 118, 6721−6732

from the M204E pellet using a variety of solvents were not successful.

Quantitative HPLC analysis also was used to assay pigment content. Fresh acetone/MeOH extract was dried under a stream of nitrogen and dissolved in the solvent mixture used for HPLC analysis (see Experimental Section). Figure S4A of the Supporting Information shows HPLC traces recorded at 770 nm. To make an absolute comparison, the analysis was performed on the same concentrations of wild-type, M204E, and a 1:1 mixture of both. The traces are very similar, and there is no difference in retention times between wild-type and mutant. The only difference is the intensity of the band around 7 min, which can be attributed to BChl. The ratio of the integrated peak areas for wild-type, M204E, and the 1:1 mixture is 4:2.7:3.3, again suggesting incomplete extraction of BChl. The amount of extracted BPh is the same for wild-type, mutant, and mix (at 16 min). Extraction methods using different solvents or solvent mixtures did not change the observation that one BChl is not extracted from M204E.

In an earlier study on a RC mutant of *Rb. sphaeroides*, in which isoleucine L177 (C_2-symmetry partner to M204) was substituted by histidine, it was proposed that one BChl might be covalently attached to the protein based on a colored polypeptide band in SDS−PAGE.[82] For the M204E mutant, no colored polypeptide band is seen in SDS−PAGE and no chromophore absorption was observed in UV/vis/NIR spectra from parts of the gel that were cut out (Figure S4B of the Supporting Information). LC−MS/MS analysis of M204E and wild-type was also used to investigate possible covalent attachment of a BChl. The mass spectra of peptide M200-M208 (HGLSEAALY) show no evidence for covalent attachment of BChl (Figure S5 of the Supporting Information). However, the blue-green pellets for M204E (compared to pale yellow for wild-type) obtained during the course of processing RCs for both the UV/vis/NIR spectroscopic, and the mass spectral pigment assays provide visual evidence that a chromophore is not being solubilized, consistent with the low BChl content obtained from the acetone:methanol extraction method. The time-resolved measurements presented in the next section give no indication of the absence of a pigment from M204E RCs and should be sensitive to such a deficiency.

Redox Titrations. In order to quantify redox potentials of the special pair (P), we performed redox titrations on both WT and the M204E mutant. The values obtained are 490 ± 9 mV and 498 ± 3 mV for WT and M204E, respectively. This indicates that the free energies of the charge-separated states (e.g., $P^+B_A^-$) in M204E are not altered due to a change in the redox potential of the BChl dimer P.

Ultrafast TA Measurements. Figures 5 and 6 show the TA spectra of M204E RCs in the near-infrared and visible regions and kinetic data and fits at select key wavelengths. The data in Figures 5A and 6 (panels A and B) were obtained with direct excitation of P at 865 nm, and the data in Figure 5B were acquired using excitation at 595 nm. The 0.5−0.6 ps spectra in Figures 5 and 6 are that of P* and are identical to P* spectra reported previously. On the red side of the bleaching of the 865 nm band of P, the TA spectra are dominated by stimulated emission from P* with only the far red-edge (~900−920 nm) of P bleaching observed in the spectra acquired at ~100 ps and longer times in Figure 5A. Decay of the stimulated emission averaged over the 10 nm interval 920−930 nm is shown in the inset of Figure 5A. This interval spans an ~925 nm isosbestic point in the P bleaching spectrum (see e.g., Figure 5B inset).

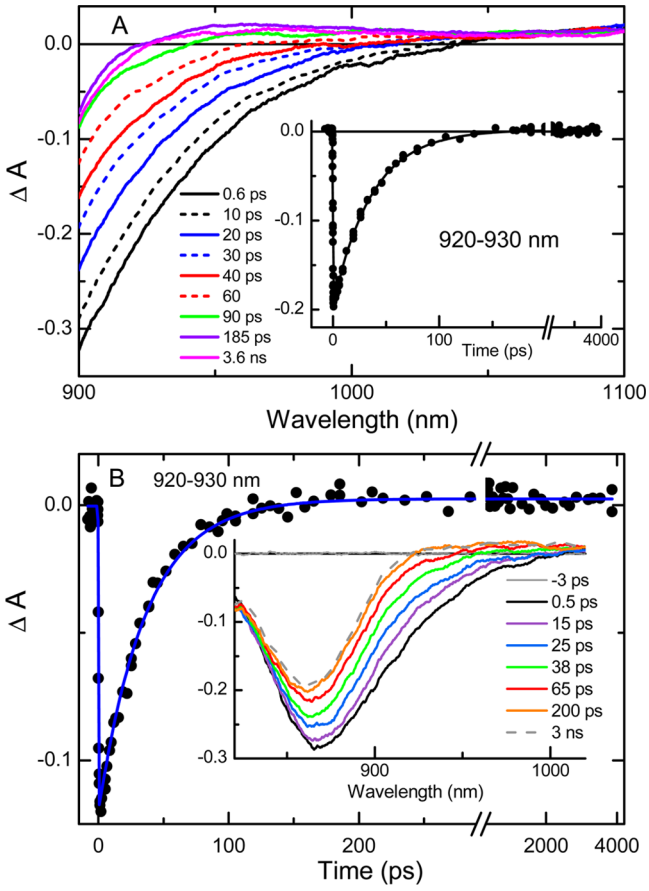

Figure 5. TA spectra and kinetics acquired with 120 fs excitation flashes at (A) 865 nm or (B) at 595 nm. In both (A and B), the kinetic data (●) are the absorption changes averaged over the 920−930 nm interval of the spectra shown in that panel. The solid lines through the kinetic data are fits to the convolution of the instrument response plus one exponential plus a constant. The time constant (P* lifetime) measured in the 920−930 nm interval is 38 ± 2 ps (panel A, inset), 38 ± 1 ps (panel B), and 36 ± 2 ps from global analysis of the spectral evolution at all wavelengths shown.

The solid line in Figure 5A inset is the fit to the convolution of the instrument response plus one exponential plus a constant (fit returns zero for the constant), giving a P* lifetime of 38 ± 2 ps. There is no indication of a second longer component to the P* stimulated emission decay at this key wavelength interval (or of a shorter component either). To this point, fitting the data to a function with two exponentials does not yield meaningful results, giving, for example, 38 ps for the values of both components. Global fitting of the data encompassing the entire spectral region shown in Figure 5A returns 36 ± 2 ps for the P* lifetime. A transient absorption band at 1017 nm that would indicate formation of a BChl anion (e.g., B_A^-) is not resolved to within a few percent yield. There is no discernible pattern of detection wavelength dependence of the kinetics.

Figure 5B inset shows time-resolved TA spectra acquired using 595 nm excitation flashes which allow probing the entire long-wavelength (Q_Y) absorption band of P. The decay kinetics in the same 920−930 nm interval are shown in the main panel of Figure 5B. The solid line is again a fit to the convolution of the instrument response plus one exponential plus a constant. The P* lifetime returned from the fit is 36 ± 1 ps and again to within a few percent, there is no indication of a second longer component to the decay kinetics at this key isosbestic point.

dx.doi.org/10.1021/jp503422c | J. Phys. Chem. B 2014, 118, 6721−6732

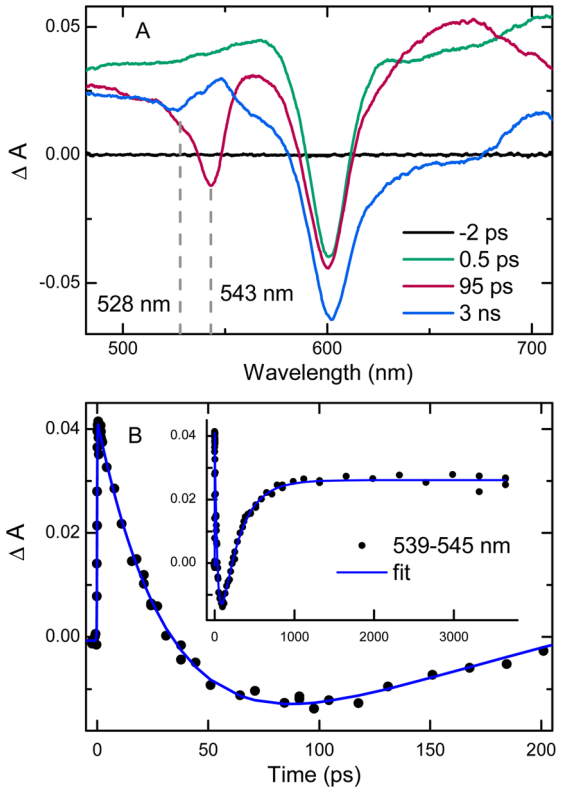

Figure 6. (A) TA spectra of M204E acquired at the times indicated following 120 fs excitation flashes at 865 nm. (B) Kinetics averaged between 539 and 545 nm (●) and fit to the instrument response plus three exponentials plus a constant. The resultant time constants are 35 ± 2 ps, 238 ± 10 ps, and 3 ns (fixed).

The spectra in Figure 5B inset show, on the blue-side of the P bleaching where stimulated emission contributes minimally, that 20−25% of P bleaching has decayed at 3 ns. Some of this occurs as P* decays, indicating internal conversion of P* to the ground state, and some of the P bleaching decay occurs on the nanosecond timescale and is associated with decay of $P^+H_B^-$, as will be described below.

The TA spectra in the visible region acquired using 865 nm flashes are shown in Figure 6A. The spectrum of P* at 0.5 ps is identical to that reported previously for wild-type and numerous mutants. The spectrum at 95 ps (nearly three 3 multiples of the P* lifetime) displays features associated with a mix of $P^+H_A^-$ and $P^+H_B^-$. The expected wavelengths for bleaching of the Q_X absorption bands are 542/543 nm (H_A) and 527/528 nm (H_B). Both such bleaching features are in evidence in the spectrum at 95 ps, with H_A bleaching dominating. The peaks of the broad anion bands of H_A and H_B are known to occur at ∼665 nm (H_A) and ∼640 nm (H_B). Again, the 95 ps spectrum displays anion absorption indicative of a mix of species but dominated by H_A^-. At 3 ns, the spectrum has largely the characteristics of $P^+Q_A^-$ (and $P^+Q_B^-$).

The data averaged between 539 and 545 nm, encompassing the maximum of the H_A bleaching, and fit to the convolution of the instrument response plus three well-separated exponentials plus a constant are shown in Figure 6B. This fit returns values of 35 ± 2 ps (assigned to P* decay) and 238 ± 10 ps (assigned to $P^+H_A^-$ decay), with a 3 ns component fixed for $P^+H_B^-$ decay. (Previous work with mutant RCs where $P^+H_B^-$ is formed and where there are no mutations in the immediate H_B and Q_B sites has found that the $P^+H_B^-$ lifetime is ∼2 or ∼4 ns in the presence or absence of Q_B, respectively.[56] Fixing this value in the present work at either 2 or 4 ns does not significantly alter the fit results; the 3 ns average value was chosen for convenience and since the Q_B occupancy is unknown.) A global fit of the data between 480 and 720 nm to the same function returns values of 36 ± 2 ps and 230 ± 15 ps with, again, the third exponential (of small amplitude) fixed at 3 ns. The ∼230 ps lifetime of $P^+H_A^-$ is identical to that measured for $P^+H_A^- \rightarrow P^+Q_A^-$ ET in wild-type RCs in Deriphat, and this assignment is made here. Analysis of the P bleaching decay kinetics on the blue side of the Q_Y band (e.g., 840−850 nm) that includes a 230 ps component does not improve the fits. We cannot rule out that the yield of $P^+H_A^- \rightarrow P^+Q_A^-$ ET might be slightly less than ∼100%.

In wild-type RCs, $P^+H_A^-$ forms in near 100% yield and bleaching of the Q_X band of H_A reaches essentially the same magnitude as the bleaching of the Q_X band of P at 600 nm. For the M204E mutant, the maximal bleaching of H_A at 543 nm reaches a much smaller maximum amplitude between 90 and 100 ps (Figure 6). This is a consequence of the long ∼35 ps P* lifetime, the reduced yield of $P^+H_A^-$, and the ∼230 ps lifetime of $P^+H_A^-$. To understand this in detail, kinetic simulations were performed and ranges of values explored for the rate constants for P* internal conversion and ET to H_A and H_B that would simultaneously reproduce the measured P* lifetime in M204E and the measured yields of charge-separated states. Six example simulations are shown in Figure S6 of the Supporting Information. The scheme in Figure 7 shows a composite

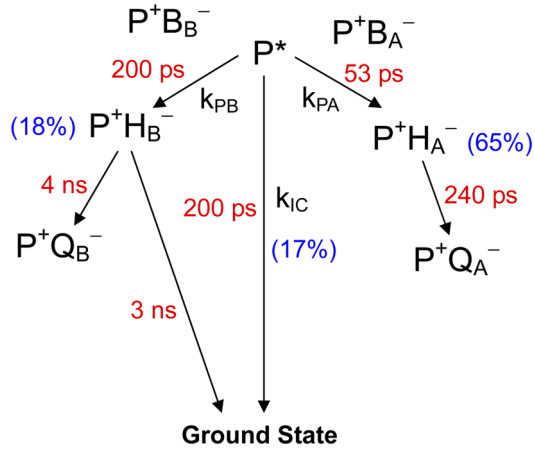

Figure 7. Photochemical model for M204E RCs. As discussed in the text, the values of the time constants for the wild-type *Rb. capsulatus* RC (and detergent) are nominally the same as those shown for the M204E RC, except the first A-side steps in WT are $P^* \rightarrow P^+B_A^- \rightarrow P^+H_A^-$ in 3 and 1 ps, respectively, with unity yield.

model that reproduces the measured P* lifetime of ∼35 ps and the measured yields of ground state and charge-separated states formed from P*. A number of studies have consistently found that the internal conversion time constant ($1/k_{IC}$) for (unperturbed) P* in *Rb. capsulatus* RCs in Deriphat-Tris buffer at 295 K falls within a range of ∼180 to 220 ps (although this value is sensitive to the environment of P, for example, being ∼100 ps in LDAO-Tris buffer[52]). Mutations that perturb P of course would be expected to affect the time constant for P* internal conversion. However, modeling with much smaller or larger time constants for P* internal conversion would result in

dx.doi.org/10.1021/jp503422c | J. Phys. Chem. B 2014, 118, 6721−6732

a respectively larger or smaller yield of ground state recovery from P* than the measured experimental value.

From previous work,[49,50] and with no mutations introduced around B_B, the time constant ($1/k_{PB}$) for (presumably superexchange mediated) P* → $P^+H_B^-$ ET is expected to be similar to that of P* internal conversion, ∼200 ps. The measured 15−20% yields for both P → ground state and P* → $P^+H_B^-$ for M204E are consistent with this, and thus the simulations explored a relatively small range (150 to 220 ps) of values for $1/k_{IC}$ and $1/k_{PB}$. Again, smaller/larger values for $1/k_{PB}$ and $1/k_{IC}$ would result in higher/lower yields of $P^+H_B^-$ and ground state recovery, inconsistent with the experimentally observed yields. In addition to reproducing the yields of the P* decay products, the values used for k_{IC}, k_{PA}, and k_{PB} must reproduce the measured ∼35 ps lifetime of P* [i.e., 35 ps = $1/(k_{IC} + k_{PB} + k_{PA})$]. From this analysis $1/k_{PA}$ is determined to be ∼50 ps and the yield of $P^+H_A^-$ is 65%. In the simulations, the maximal transient buildup of $P^+H_A^-$ is only 40−45% and this occurs at 90−100 ps. This is in excellent agreement with the experimentally observed time course of H_A bleaching, attaining maximal amplitude between 90 and 100 ps (Figure 6B). Other points of agreement between the experimental data, the simulations, and composite model in Figure 7 include the amount of P* that decays to the ground state by internal conversion (mentioned above) and the magnitude of P bleaching observed at 3−4 ns.

As a further check of the model in Figure 7, we set the challenge to reproduce the experimentally observed TA spectrum at 100 ps using the known basis spectra of the species involved. The TA spectrum of each individual state P*, $P^+H_A^-$, and $P^+Q_A^-$, the latter two both at ∼100% yield with respect to P*, are known with high fidelity from extensive studies on wild-type RCs. The TA spectrum of $P^+Q_B^-$ can be equated to that of $P^+Q_A^-$. The TA spectrum of state $P^+H_B^-$ is also known, in this case from a mutant in which this state forms in 70% yield as the sole ET product of P* decay (200 ps internal conversion accounting for the remaining 30% P* decay pathway).[52] Thus, we have the basis TA spectra needed to reproduce the TA spectrum at 100 ps (or at any other time). Figure 8 compares the experimental (red) and calculated (simulated) TA spectrum at 100 ps, and the agreement is excellent. The calculated spectrum in blue is the following sum of the known TA basis spectra: 9% P* + 48% $P^+H_A^-$ + 15% $P^+H_B^-$ + 15% $P^+Q_A^-$ + 1% $P^+Q_B^-$ + 12% ground state (no TA change). The percentages of these species present at 100 ps were based on the kinetic simulations (Figure S6 of the Supporting Information). Beer's law holds here, requiring that the simulation quantitatively reproduce the TA changes referenced to the initial concentration of P* produced upon excitation. In other words, the simulation must replicate not only shapes of spectral features but also the absolute magnitude of the absorption changes and such are achieved in Figure 8.

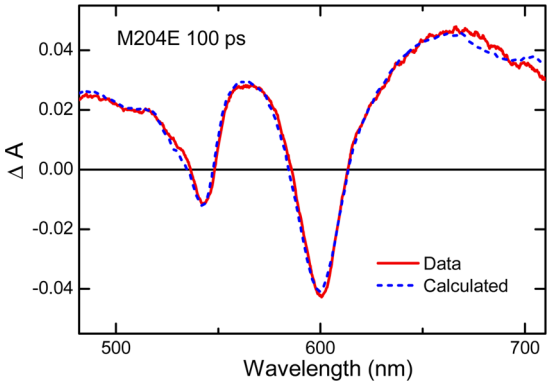

Figure 8. Experimental TA spectrum of M204E RCs acquired 100 ps following excitation with ∼120 excitation flashes at 865 nm (red). The blue TA spectrum at 100 ps is calculated from the basis set of the TA spectra of P* and the charge separated states. See text for details.

DISCUSSION

In the following, we place the unusually straightforward and homogeneous kinetics observed for the M204E mutant in the context of many attempts to understand the connection between energetics and kinetics in RCs, which in most cases are considerably more complex. Glutamic acid at M204 introduces into the environment of the conserved Tyr M208 a residue with the potential to hydrogen bond to the Tyr hydroxyl group and change its positioning with respect to B_A. Theoretical work predicts that reorienting the Tyr −OH can significantly raise the free energy of $P^+B_A^-$ and impede A-side charge separation.[8] The work presented here develops these ideas. First, an NMR signal analogous to one previously assigned in studies of wild-type *Rb. sphaeroides* RCs to a nonhydrogen bonded Tyr M210 residue[45,46] is present in the NMR spectrum of wild-type *Rb. capsulatus* but absent from the NMR spectrum of the *Rb. capsulatus* M204E mutant RC (Figure 3). Hydrogen bonded or not, the NMR data clearly indicate that the introduced glutamic acid has significantly affected the environment of Tyr M208. Ultrafast measurements reveal that this single amino acid change has substantial effects on charge separation. Electron transfer from P* to H_A is about a factor of 10 slower than in wild-type and $P^+H_A^-$ no longer forms in 100% yield. Specifically, the P* lifetime is ∼35 ps and P* decays via ∼50 ps ET to H_A (∼65% yield) and via ET to H_B and internal conversion to the ground state with about equal time constants (∼200 ps) and yields (17−18%) for both, as in Figure 7.

In broad view, the M204E mutant has parallels to two *Rb. sphaeroides* mutants that bear a single amino acid change and result in a similar P* lifetime. Replacing the conserved Tyr M210 in *Rb. sphaeroides* with Trp results in P* having an ∼40 ps lifetime but heterogeneous kinetics.[11,21,39] Replacing the native Gly at M203 with Leu in *Rb. sphaeroides* (equivalent of M201 in *Rb. capsulatus*) also results in a long ∼40 ps P* lifetime.[83] The crystal structure of the M203L mutant[83] reveals steric exclusion of a water molecule, denoted water-A, that in the wild-type crystal structures (Figure 2) is positioned such that it could form a hydrogen-bond bridge between His M202 (in *Rb. sphaeroides* the axial ligand to the Mg of one macrocycle of P) and the ring-V keto group of B_A.[1,2] These three mutants provide glimpses into potential multiple molecular interactions that may stabilize and fine-tune the free energy of $P^+B_A^-$: the presence of a Tyr near B_A, optimal orientation of the Tyr hydroxyl group with respect to B_A, and a hydrogen bond to the ring-V keto group of B_A. For all three mutants, $P^+B_A^-$ is suggested to be sufficiently destabilized that it is above P*, thereby lengthening by 10-fold the P* lifetime.

Electron transfer in the M204E mutant is consistent with prior work on a still relatively small family of *Rb. capsulatus* mutants in which P* decay is partitioned fairly straightforwardly between significant yields (more than just a few percent) of internal conversion and ET to H_B along with A-side ET. Many, but not all, of these mutant RCs employ a Tyr at

dx.doi.org/10.1021/jp503422c | J. Phys. Chem. B 2014, 118, 6721−6732

L181 (which presumably lowers the free energy of $P^+B_B^-$) and a Phe at M208. However, in M204E, the native Tyr M208 and Phe L181 are unchanged, as they were in the first two mutants in which ET to the B-side was observed, namely the "DH" and "KDH" mutants[47,84] [where DH = G(M201)D+L(M212)H and KDH = S(L178)K+DH]. For ease of observing H_B bleaching unambiguously, in many of the "wrong way" mutants the Leu at M212 is changed to a His, which results in a BChl, denoted β, in place of H_A.[85] However, this is not the case in M204E or the "YF" mutant[49] (swap of L181 Phe to Tyr and of M208 Tyr to Phe) or in mutants in which there is no pigment in the H_A site (D_{LL} mutants[52−54]) or no pigment in the B_A site (M204Q mutants[55]).

Among these mutants, the detergent used to solubilize *Rb. capsulatus* RCs has been observed to exert a consistent influence. Specifically, Deriphat 160-C and LDAO impart different photophysical properties to P* and the rates of its decay pathways. Not considering mutants aimed specifically at affecting the dimer, the long-wavelength absorption band of P usually occurs near 850 nm for *Rb. capsulatus* RCs in LDAO:Tris buffer but usually is at 865 nm in Deriphat:Tris buffer, the latter essentially the same as found when the (wild-type) RC resides in its native membrane. For both wild-type and the L(M212)H ("beta") mutant, the P* lifetime in Deriphat:Tris buffer is about double that found for these RCs in LDAO-Tris buffer.[50] Similarly, the time constant for internal conversion of P* is about a factor of 2 larger for RCs solubilized in Deriphat (200 ps) than in LDAO (100 ps). Although this was apparent during early work,[49,50] it was underscored in the recently revived D_{LL} mutant,[52] first made in the Youvan lab ca. 1990,[86,87] wherein P* decays solely (100%) by internal conversion to the ground state. The recent work established that the time constant for this process at room temperature is ∼200 ps for *Rb. capsulatus* RCs in Deriphat:Tris buffer and ∼100 ps for RCs in LDAO:Tris buffer.[52]

The D_{LL} (H_A-less) mutant has provided basis for understanding a 200 ps component of biexponential P* stimulated emission decay sometimes found in *Rb. capsulatus* mutants in Deriphat:Tris buffer where the goal has been to manipulate the free energies of the A- and B-side charge-separated states. The amplitude of the 200 ps stimulated emission component has generally ranged between 20 and 40%. Meanwhile, a second, and shorter kinetic component is measured for P* stimulated emission decay and measured at wavelengths associated with reduction of electron acceptors (e.g., H_A/β and H_B). However, the ∼200 ps kinetic component is not measured at wavelengths associated with reduction of electron acceptors, rather only at the wavelengths of P* stimulated emission and P bleaching. These results have indicated that attempts to favor ET to the B side (by lowering the free energy of $P^+B_B^-$) and disfavor ET to the A side (by raising the free energy of $P^+B_A^-$) can (and often do) give rise to a 20−40% population of "inactive" RCs in which charge separation does not occur (or is substantially impeded).[50,54,55] For this "inactive" population, P* has an ∼200 ps lifetime and decays as in D_{LL} by internal conversion to the ground state (or ∼100 ps for RCs in the LDAO:Tris buffer).

The M204E mutant studied here is nearly unique for a *Rb. capsulatus* RC in Deriphat, having a (relatively) long P* lifetime and an absence of a population of RCs in which ET does not occur. Another such case is the *Rb. capsulatus* D_{LL}-1 variant (formerly denoted D_{LL}-FY_LF_M in ref 52), in which P* decays at room temperature with single exponential kinetics (to within a few percent), as discussed further below. P* populations in which differing rates of ET and even differing photochemistry occur are likely rooted in the following inter-related factors. (i) In the native RC, the five key electronic states for initial charge separation (P*, $P^+B_A^-$, $P^+B_B^-$, $P^+H_A^-$, and $P^+H_B^-$) span a modest ∼0.5 eV in free energy. (ii) The mutants designed to influence the primary events aim to shift the free energies of one or more states and likely compress this span by as much as a factor of 2. This results in very small spacings between any of these states and especially between P* and $P^+B_A^-$ and $P^+B_B^-$. Additionally, many mutants employ the L(M212)H mutation (M214 in *Rb. sphaeroides*) and $P^+\beta^-$ is estimated to be ∼150 to 200 meV higher in free energy than $P^+H_A^-$, placing it essentially isoenergetic with (wild-type) $P^+B_A^-$. (iii) Such small energy spacing makes the rates, yields, and directionality of charge separation very sensitive to different RC or P* "conformations" or "populations" that represent a natural landscape of cofactor, protein interactions, static, dynamic, or both. Heterogeneous kinetics in wild-type RCs have been ascribed to pigment/protein conformers or populations[66,88] and links between protein dynamics and ET have been much discussed.[29,64,89] The presence, position, and orientation of water molecules may contribute,[1,2] such as one ("water-A") that may bridge the His (M202, equiv of M200 in *Rb. capsulatus*) ligand on P_M and B_A via hydrogen bonds, and that has been the subject of much recent study.[32,83,90−94] Additionally for *Rb. capsulatus* RCs, P* is ∼26 meV lower in free energy in Deriphat than in LDAO, which is ∼25% of the estimated free-energy difference between P* and $P^+B_A^-$. This makes even more plausible the differences found between the P* lifetimes for some *Rb. capsulatus* RCs in Deriphat versus LDAO or for differences between membrane-bound RCs versus RCs in detergent micelles.

The results obtained here for the *Rb. capsulatus* M204E RC resonate with these themes. This mutant was designed to potentially reposition the hydroxyl group of Tyr M208 nearly in an orientation postulated to maximally destabilize $P^+B_A^-$ in free energy and thus impede the critical first step of $P^* \rightarrow P^+B_A^- \rightarrow P^+H_A^-$ primary charge separation. The calculations of Alden et al.[8] indicated that in wild-type RCs, the M208 Tyr −OH group is confined to an orientation that lowers the free energy of $P^+B_A^-$ by as much as ∼200 meV (∼40 meV of this is an effect on the P oxidation potential). Our modeling of possible interactions between a Glu at M204 and a Tyr at M208 indicates that if a hydrogen bond forms between these residues, the Tyr hydroxyl group could be rotated ∼120° away from the ideal geometry found by Alden et al. and only ∼60° from a geometry that provides the least free energy stabilization of $P^+B_A^-$. Given that $P^+B_A^-$ is thought to be only 50−100 meV below P* in wild-type, it is plausible that this state is higher in free energy than P* in M204E (Figure 7). (Note that the energetic consequences of the Tyr-OH dipole being hydrogen bonded to a glutamic acid were not modeled in Alden et al.[8]) We cannot know with certainty that the hydroxyl group of Tyr M208 is hydrogen bonded to the glutamic acid introduced at M204, but the NMR spectrum is consistent with this and minimally shows that the −OH of Tyr M208 (and/or the entire residue) experiences a different environment. In addition or alternatively, depending on the side chain position and ionization state, a Glu at M204 could directly or indirectly affect B_A, P, or "water-A", changing interactions between them or other cofactors. The functional consequence remains that $P^* \rightarrow P^+H_A^-$ ET has an ∼50 ps time constant (and ∼65% yield), allowing the relatively slow native ∼200 ps time constants for

dx.doi.org/10.1021/jp503422c | J. Phys. Chem. B 2014, 118, 6721−6732

ET to H_B and internal conversion of P* to the ground state to compete.

Additionally, and somewhat unusually, the P* decay kinetics in M204E are quite homogeneous with no discernible contribution of an ∼200 ps (or other) component in the P* stimulated emission decay kinetics and no discernible detection wavelength dependence to the P* decay kinetics. Thus, not only is an "inactive" population absent, the data indicate only a comparatively narrow (or no) distribution of P* functional forms. Even for D_{LL} RCs, where again P* decays solely by internal conversion, a 3-fold wide distribution of P* decay time constants spanning several hundred picoseconds is found at 77 K in both LDAO and Deriphat.[53] The absence of detection-wavelength dependent kinetics in the M204E mutant may indirectly signal, or at least be consistent with, the introduced glutamic acid negating or constraining some pigment or protein native motions (conformational changes or rotomers) as might result, for example, upon formation of a hydrogen bond between Glu M204 and the −OH group of Tyr M208.

Some final connections can be made to two other D_{LL} variants,[54] ones that led to our making M204E in the first place. In both of these mutants, P* decay was found to be biexponential, but instead of one photochemically "active" P* population and an "inactive" P* population with an ∼200 ps lifetime there were two distinct "active" P* populations. In one, P* decayed with an ∼10 ps time constant and gave rise to formation of $P^+B_A^-$, which state lived for ∼300 ps and was trapped because H_A is absent from all RCs in the D_{LL} mutant family. In the second population, P* had an ∼100 ps lifetime and decayed via a combination of ET to H_B and internal conversion to the ground state. The D_{LL} motif bears a number of changes around the A-side cofactors, including having a Phe at M208. In the D_{LL} variants where $P^+B_A^-$ was trapped, M208 was restored to a Tyr, and we speculated whether the two populations might reflect orientations of Tyr at M208. The M204E RC was born of the idea of whether it might be possible to pin down Tyr M208 and affect the populations.

The simple scheme shown in Figure 7, where both $P^+B_A^-$ and $P^+B_B^-$ are placed higher than P*, suggests that in M204E P* → $P^+H_A^-$ ET occurs not by a two-step processes wherein $P^+B_A^-$ is a chemical intermediate but rather occurs in a manner posited for P* → $P^+H_B^-$ ET. All cases of P* → $P^+H_B^-$ to date, even aided by a Tyr at L181, are presumed to occur with superexchange assistance of $P^+B_B^-$. Depending on the mutations involved, the time constant for P* → $P^+H_B^-$ ET has ranged from ∼70 to ∼200 ps; again, these values are for various mutants in Deriphat and ∼40 ps, the smallest time constant obtained, is for a mutant in LDAO. Interestingly, the ∼50 ps time constant for P* → $P^+H_A^-$ ET in M204E is within this range. On the B-side, the smaller values in a 100−200 ps range of time constants have been achieved with a Tyr residue at L181 with 200 ps the case for the native Phe.

Electron transfer in the M204E mutant thus conforms well compared to prior observations and analyses. It appears that in this interesting mutant, the free energy of $P^+B_A^-$ is significantly affected (likely raised above P*), and the balance of ET in the RC is disrupted even though the native, key Tyr at M208 is in place. Even though the P* lifetime is a very long ∼35 ps, $P^+H_A^-$ is still the dominant product of P* decay, though reduced to ∼65% yield. The native Phe at L181 also is in place, and the time constant for P* → $P^+H_B^-$ is unchanged from the ∼200 ps value (for *Rb. capsulatus* in Deriphat) that has been repeatedly found for mutants with a (presumably) "native" B-side but in which ET to H_B is observed because of impeded A-side ET. Similarly, the time constant for P* internal conversion is unchanged from the "native" ∼200 ps (again, the value for *Rb. capsulatus* in Deriphat). Finally, P* decay in M204E appears to occur fairly uniformly in the entire RC or P* population. This suggests a P* "population" in which $P^+B_A^-$ is elevated well out of the small, congested free-energy window normally occupied by all five key electronic states, whose free energy spacing/ordering is highly sensitive to static/dynamic protein effects that drive the relative contributions of the three P* decay pathways, which give ET to the A-side, ET to the B-side, or no ET at all.

■ ASSOCIATED CONTENT

Supporting Information

Material related to optimal growth conditions of *Rb. capsulatus* cultures, RC pigment content analysis, and kinetic simulations of P* decay is provided. This material is available free of charge via the Internet at http://pubs.acs.org.

■ AUTHOR INFORMATION

Corresponding Author

*E-mail: kirmaier@wustl.edu. Tel: 314-935-6480. Fax: 314-935-4481.

Present Address

[§]Miguel Saggu is presently affiliated with Late Stage Pharmaceutical Development, Genentech, 1 DNA Way, South San Francisco, CA 94080.

Notes

The authors declare no competing financial interest.

■ ACKNOWLEDGMENTS

This research was supported by grants from the National Science Foundation to C.K. and D.H. (MCB-0948996) and to S.G.B. (MCB-0918782). L.C. acknowledges support from the NIH Director's New Innovator Award Program (DP2OD007488) and the Stanford Terman Fellowship. M.S. was funded by a DFG Forschungsstipendium (Deutsche Forschungsgemeinschaft, Sa 2156/1-1). X.Z. is the recipient of a Stanford Interdisciplinary Graduate Fellowship. Christopher Adams from the Stanford University mass spectrometry facility is acknowledged for his support with the LC−MS/MS.

■ REFERENCES

(1) Ermler, U.; Fritsch, G.; Buchanan, S. K.; Michel, H. Structure of the Photosynthetic Reaction Centre from *Rhodobacter sphaeroides* at 2.65 A Resolution: Cofactors and Protein-Cofactor Interactions. *Structure* **1994**, *2*, 925−936.

(2) Ermler, U.; Michel, H.; Schiffer, M. Structure and Function of the Photosynthetic Reaction-Center from Rhodobacter-Sphaeroides. *J. Bioenerg. Biomembr.* **1994**, *26*, 5−15.

(3) Koepke, J.; Krammer, E. M.; Klingen, A. R.; Sebban, P.; Ullmann, G. M.; Fritzsch, G. pH Modulates the Quinone Position in the Photosynthetic Reaction Center from *Rhodobacter sphaeroides* in the Neutral and Charge Separated States. *J. Mol. Biol.* **2007**, *371*, 396−409.

(4) Parson, W. W.; Chu, Z. T.; Warshel, A. Electrostatic Control of Charge Separation in Bacterial Photosynthesis. *Biochim. Biophys. Acta* **1990**, *1017*, 251−272.

(5) Bixon, M.; Jortner, J.; Michel-Beyerle, M. E. On the Mechanism of Primary Charge Separation in Bacterial Photosynthesis. *Biochim. Biophys. Acta* **1991**, *1056*, 301−315.

(6) Blomberg, M. R. A.; Siegbahn, P. E. M.; Babcock, G. T. Modeling Electron Transfer in Biochemistry. A Quantum Chemical Study of

Charge Separation in *Rhodobacter sphaeroides* and Photosystem II. *J. Am. Chem. Soc.* **1998**, *120*, 8812−8824.
(7) Alden, R. G.; Parson, W. W.; Chu, Z. T.; Warshel, A. Calculations of Electrostatic Energies in Photosynthetic Reaction Centers. *J. Am. Chem. Soc.* **1995**, *117*, 12284−12298.
(8) Alden, R. G.; Parson, W. W.; Chu, Z. T.; Warshel, A. Orientation of the OH Dipole of Tyrosine (M)210 and Its Effect on Electrostatic Energies in Photosynthetic Bacterial Reaction Centers. *J. Phys. Chem.* **1996**, *100*, 16761−16770.
(9) Gunner, M. R.; Nicholls, A.; Honig, B. Electrostatic Potentials in *Rhodopseudomonas viridis* Reaction Centers: Implications for the Driving Force and Directionality of Electron Transfer. *J. Phys. Chem.* **1996**, *100*, 4277−4291.
(10) Hughes, J. M.; Hutter, M. C.; Reimers, J. R.; Hush, N. S. Modeling the Bacterial Photosynthetic Reaction Center. 4. The Structural, Electrochemical, And Hydrogen-Bonding Properties of 22 Mutants of Rhodobacter sphaeroides. *J. Am. Chem. Soc.* **2001**, *123*, 8550−8563.
(11) Nagarajan, V.; Parson, W. W.; Gaul, D.; Schenck, C. Effect of Specific Mutations of Tyrosine-(M)210 on the Primary Photosynthetic Electron-Transfer Process in Rhodobacter-Sphaeroides. *Proc. Natl. Acad. Sci. U.S.A.* **1990**, *87*, 7888−7892.
(12) Finkele, U.; Lauterwasser, C.; Zinth, W.; Gray, K. A.; Oesterhelt, D. Role of Tyrosine M210 in the Initial Charge Separation of Reaction Centers of *Rhodobacter sphaeroides*. *Biochemistry* **1990**, *29*, 8517−8521.
(13) Chan, C.-K.; Chen, L. X.-Q.; DiMagno, T. J.; Hanson, D. K.; Nance, S. L.; Schiffer, M.; Norris, J. R.; Fleming, G. R. Initial Electron Transfer in Photosynthetic Reaction Centers of *Rhodobacter capsulatus* Mutants. *Chem. Phys. Lett.* **1991**, *176*, 366−372.
(14) Gray, K. A.; Wachtveitl, J.; Oesterhelt, D. Photochemical Trapping of a Bacteriopheophytin Anion in Site-Specific Reaction Center Mutants from the Photosynthetic Bacterium *Rhodobacter sphaeroides*. *Eur. J. Biochem.* **1992**, *207*, 723−731.
(15) Schiffer, M.; Chan, C.-K.; Chang, C.-H.; DiMagno, T. J.; Fleming, G. R.; Nance, S.; Norris, J. R.; Synder, S.; Thurnauer, M.; Tiede, D. M.; Hanson, D. K. Study of Reaction Center Function by Analysis of the Effects of Site-Specific and Compensatory Mutations. In *The Photosynthetic Bacterial Reaction*; Center, I. I., Breton, J., Vermeglio, A., Eds.; Plenum: New York, 1992; pp 351−361.
(16) Du, M.; Rosenthal, S. J.; Xie, X.; DiMagno, T. J.; Schmidt, M.; Hanson, D. K.; Schiffer, M.; Norris, J. R.; Fleming, G. R. Femtosecond Spontaneous-Emission Studies of Reaction Centers from Photosynthetic Bacteria. *Proc. Natl. Acad. Sci. U.S.A.* **1992**, *89*, 8517−8521.
(17) Nagarajan, V.; Parson, W. W.; Davis, D.; Schenck, C. C. Kinetics and Free Energy Gaps of Electron Transfer Reactions in *Rhodobacter sphaeroides* Reaction Centers. *Biochemistry* **1993**, *32*, 12324−12336.
(18) Jia, Y.; DiMagno, T. J.; Chan, C.-K.; Wang, Z.; Du, M.; Hanson, D. K.; Schiffer, M.; Norris, J. R.; Fleming, G. R.; Popov, M. S. Primary Charge Separation in Mutant Reaction Centers of *Rhodobacter capsulatus*. *J. Phys. Chem.* **1993**, *97*, 13180−13191.
(19) Hamm, P.; Gray, K. A.; Oesterhelt, D.; Feick, R.; Scheer, H.; Zinth, W. Subpicosecond Emission Studies of Bacterial Reaction Centers. *Biochim. Biophys. Acta* **1993**, *1142*, 99−105.
(20) Jones, M. R.; Heer-Dawson, M.; Mattioli, T. A.; Hunter, C. N.; Robert, B. Site-Specific Mutagenesis of the Reaction Centre from Rhodoacter sphaeroides Studied by Fourier Transform Raman Spectroscopy: Mutations at Tryosine M210 Do Not Affect the Electronic Structure of the Primary Donor. *FEBS Lett.* **1994**, *339*, 18−24.
(21) Shochat, S.; Arlt, T.; Francke, C.; Gast, P.; Vannoort, P. I.; Otte, S. C. M.; Schelvis, H. P. M.; Schmidt, S.; Vijgenboom, E.; Vrieze, J.; Zinth, W.; Hoff, A. J. Spectroscopic Characterization of Reaction Centers of the (M)Y210W Mutant of the Photosynthetic Bacterium Rhodobacter-Sphaeroides. *Photosynth. Res.* **1994**, *40*, 55−66.
(22) Beekman, L. M. P.; van Stokkum, I. H. M.; Monshouwer, R.; Rijnders, A. J.; McGlynn, P.; Visschers, R. W.; Jones, M. R.; van Grondelle, R. Primary Electron Transfer in Membrane-Bound Reaction Centers with Mutations at the M210 Position. *J. Phys. Chem.* **1996**, *100*, 7256−7268.
(23) Laible, P. D.; Greenfield, S. R.; Wasielewski, M. R.; Hanson, D. K.; Pearlstein, R. M. Antenna Excited State Decay Kinetics Establish Primary Electron Transfer in Reaction Centers as Heterogeneous. *Biochemistry* **1997**, *36*, 8677−8685.
(24) Streltsov, A. M.; Vulto, S. I. E.; Shkuropatov, A. Y.; Hoff, A. J.; Aartsma, T. J.; Shuvalov, V. A. B_A and B_B Absorbance Perturbations Induced by Coherent Nuclear Motions in Reaction Centers from Rhodobacter sphaeroides upon 30-fs Excitation of the Primary Donor. *J. Phys. Chem. B* **1998**, *102*, 7293−7298.
(25) DiMagno, T. J.; Laible, P. D.; Reddy, N. R.; Small, G. J.; Norris, J. R.; Schiffer, M.; Hanson, D. K. Protein-Chromophore Interactions: Spectral Shifts Report the Consequences of Mutations in the Bacterial Photosynthetic Reaction Center. *Spectrochim. Acta, Part A* **1998**, *54*, 1247−1267.
(26) Zhou, H.; Boxer, S. G. Probing Excited-State Electron Transfer by Resonance Stark Spectroscopy. 2. Theory and Application. *J. Phys. Chem. B* **1998**, *102*, 9148−9160.
(27) McAuley, K. E.; Fyfe, P. K.; Cogdell, R. J.; Isaacs, N. W.; Jones, M. R. X-ray Crystal Structure of the YM210W Mutant Reaction Centre from *Rhodobacter sphaeroides*. *FEBS Lett.* **2000**, *467*, 285−290.
(28) de Boer, A. L.; Neerken, S.; de Wijn, R.; Permentier, H. P.; Gast, P.; Vijgenboom, E.; Hoff, A. J. B-Branch Electron Transfer in Reaction Centers of Rhodobacter sphaeroides Assessed with Site-Directed Mutagenesis. *Photosynth. Res.* **2002**, *71*, 221−239.
(29) Guo, Z.; Woodbury, N. W.; Pan, J.; Lin, S. Protein Dielectric Environment Modulates the Electron-Transfer Pathway in Photosynthetic Reaction Centers. *Biophys. J.* **2012**, *103*, 1979−1988.
(30) Laible, P. D.; Chynwat, V.; Thurnauer, M. C.; Schiffer, M.; Hanson, D. K.; Frank, H. A. Protein Modifications Affecting Triplet Energy Transfer in Bacterial Photosynthetic Reaction Centers. *Biophys. J.* **1998**, *74*, 2623−2637.
(31) Vos, M. H.; Jones, M. R.; Breton, J.; Lambry, J. C.; Martin, J. L. Vibrational Dephasing of Long- And Short-Lived Primary Donor Excited States in Mutant Reaction Centers of Rhodobacter sphaeroides. *Biochemistry* **1996**, *35*, 2687−2692.
(32) Yakovlev, A. G.; Vasilieva, L. G.; Shkuropatov, A. Y.; Bolgarina, T. I.; Shkuropatova, V. A.; Shuvalov, V. A. Mechanism of Charge Separation and Stabilization of Separated Charges in Reaction Centers of Chloroflexus aurantiacus and of YM210W(L) Mutants of Rhodobacter sphaeroides Excited by 20 fs Pulses at 90 K. *J. Phys. Chem. A* **2003**, *107*, 8330−8338.
(33) Beekman, L. M. P.; Vanmourik, F.; Jones, M. R.; Visser, H. M.; Hunter, C. N.; Vangrondelle, R. Trapping Kinetics in Mutants of the Photosynthetic Purple Bacterium Rhodobacter-Sphaeroides: Influence of the Charge Separation Rate and Consequences for the Rate-Limiting Step in the Light-Harvesting Process. *Biochemistry* **1994**, *33*, 3143−3147.
(34) Chirino, A. J.; Lous, E. J.; Huber, M.; Allen, J. P.; Schenck, C. C.; Paddock, M. L.; Feher, G.; Rees, D. C. Crystallographic Analysis of Site-Directed Mutants of the Photosynthetic Reaction Center from *Rhodobacter sphaeroides*. *Biochemistry* **1994**, *33*, 4584−4593.
(35) Mattioli, T. A.; Gray, K. A.; Lutz, M.; Oesterhelt, D.; Robert, B. Resonance Raman Characterization of Rhodobacter-Sphaeroides Reaction Centers Bearing Site-Directed Mutations at Tyrosine M210. *Biochemistry* **1991**, *30*, 1715−1722.
(36) Gibasiewicz, K.; Pajzderska, M.; Dobek, A.; Karolczak, J.; Burdzinski, G.; Brettel, K.; Jones, M. R. Analysis of the Temperature-Dependence of P+HA- Charge Recombination in the Rhodobacter sphaeroides Reaction Center Suggests Nanosecond Temperature-Independent Protein Relaxation. *Phys. Chem. Chem. Phys.* **2013**, *15*, 16321−16333.
(37) Gibasiewicz, K.; Pajzderska, M.; Karolczak, J.; Burdzinski, G.; Dobek, A.; Jones, M. R. Primary Electron Transfer Reactions in Membrane-Bound Open and Closed Reaction Centers from Purple Bacterium Rhodobacter sphaeroides. *Acta Phys. Pol., A* **2012**, *122*, 263−268.
(38) Van Brederode, M. E.; Jones, M. R.; Van Grondelle, R. Fluorescence Excitation Spectra of Membrane-Bound Photosynthetic Reaction Centers of Rhodobacter sphaeroides in Which the Tyrosine

M210 Residue is Replaced by Tryptophan: Evidence for a New Pathway of Charge Separation. *Chem. Phys. Lett.* **1997**, *268*, 143−149.
(39) Pawlowicz, N. P.; van Stokkum, I. H. M.; Breton, J.; van Grondelle, R.; Jones, M. R. An Investigation of Slow Charge Separation in a Tyrosine M210 to Tryptophan Mutant of the Rhodobacter sphaeroides Reaction Center by Femtosecond Mid-Infrared Spectroscopy. *Phys. Chem. Chem. Phys.* **2010**, *12*, 2693−2705.
(40) Frolov, D.; Marsh, M.; Crouch, L. I.; Fyfe, P. K.; Robert, B.; van Grondelle, R.; Hadfield, A.; Jones, M. R. Structural and Spectroscopic Consequences of Hexacoordination of a Bacteriochlorophyll Cofactor in the Rhodobacter sphaeroides Reaction Center. *Biochemistry* **2010**, *49*, 1882−1892.
(41) Yakovlev, A. G.; Vasilieva, L. G.; Shkuropatov, A. Y.; Shuvalov, V. A. Primary Processes of Charge Separation in Reaction Centers of YM210L/FM197Y and YM210L Mutants of Rhodobacter sphaeroides. *Biochemistry (Moscow)* **2009**, *74*, 1203−1210.
(42) Treynor, T. P.; Yoshina-Ishii, C.; Boxer, S. G. Probing Excited-State Electron Transfer by Resonance Stark Spectroscopy: 4 Mutations near B_L in Photosynthetic Reaction Centers Perturb Multiple Factors That Affect $B_L^* \rightarrow B_L^+H_L^-$. *J. Phys. Chem. B* **2004**, *108*, 13523−13535.
(43) van der Vos, R.; Franken, E. M.; Sexton, S. J.; Shochat, S.; Gast, P.; Hore, P. J.; Hoff, A. J. Optically Detected Magnetic-Field Effects on Reaction Centers of Rhodobacter-Sphaeroides-2.4.1 and Its Tyr M210-]Trp Mutant. *Biochim. Biophys. Acta* **1995**, *1230*, 51−61.
(44) Beekman, L. M. P.; vanStokkum, I. H. M.; Monshouwer, R.; Rijnders, A. J.; McGlynn, P.; Visschers, R. W.; Jones, M. R.; vanGrondelle, R. Primary Electron Transfer in Membrane-Bound Reaction Centers with Mutations at the M210 Position. *J. Phys. Chem.* **1996**, *100*, 7256−7268.
(45) Fischer, M. R.; Degroot, H. J. M.; Raap, J.; Winkel, C.; Hoff, A. J.; Lugtenburg, J. C-13 Magic Angle Spinning NMR-Study of the Light-Induced and Temperature-Dependent Changes in Rhodobacter-Sphaeroides R26 Reaction Centers Enriched in [4′-C-13]Tyrosine. *Biochemistry* **1992**, *31*, 11038−11049.
(46) Shochat, S.; Gast, P.; Hoff, A. J.; Boender, G. J.; Vanleeuwen, S.; Vanliemt, W. B. S.; Vijgenboom, E.; Raap, J.; Lugtenburg, J.; Degroot, H. J. M. C-13 Mas NMR Evidence for a Homogeneously Ordered Environment of Tyrosine-M210 in Reaction Centers of Rhodobacter-Sphaeroides. *Spectrochim. Acta, Part A* **1995**, *51*, 135−144.
(47) Heller, B. A.; Holten, D.; Kirmaier, C. Control of Electron Transfer to the L-side Versus the M-side of the Photosynthetic Reaction Center. *Science* **1995**, *269*, 940−945.
(48) Kirmaier, C.; He, C.; Holten, D. Manipulating the Direction of Electron Transfer in the Bacterial Reaction Center by Swapping Phe for Tyr Near $BChl_M$ (L181) and Tyr for Phe Near $BChl_L$ (M208). *Biochemistry* **2001**, *40*, 12132−12139.
(49) Kirmaier, C.; Laible, P. D.; Hanson, D. K.; Holten, D. B-Side Electron Transfer to Form $P^+H_B^-$ in Reaction Centers from the F(L181)Y/Y(M208)F Mutant of *Rhodobacter capsulatus*. *J. Phys. Chem. B* **2004**, *108*, 11827−11832.
(50) Kirmaier, C.; Laible, P. D.; Hinden, E.; Hanson, D. K.; Holten, D. Detergent Effects on Primary Charge Separation in Wild-Type and Mutant *Rhodobacter capsulatus* Reaction Centers. *Chem. Phys.* **2003**, *294*, 305−318.
(51) Paddock, M. L.; Chang, C.; Xu, Q.; Abresch, E. C.; Axelrod, H. L.; Feher, G.; Okamura, M. Y. Quinone (Q_B) Reduction by B-Branch Electron Transfer in Mutant Bacterial Reaction Centers from Rhodobacter sphaeroides: Quantum Efficiency and X-ray Structure. *Biochemistry* **2005**, *44*, 6920−6928.
(52) Chuang, J. I.; Boxer, S. G.; Holten, D.; Kirmaier, C. High Yield of M-side Electron Transfer in Mutants of Rhodobacter capsulatus Reaction Centers Lacking the L-Side Bacteriopheophytin. *Biochemistry* **2006**, *45*, 3845−3851.
(53) Chuang, J. I.; Boxer, S. G.; Holten, D.; Kirmaier, C. Temperature Dependence of Electron Transfer to the M-Side Bacteriopheophytin in *Rhodobacter capsulatus* Reaction Centers. *J. Phys. Chem. B* **2008**, *112*, 5487−5499.
(54) Carter, B.; Boxer, S. G.; Holten, D.; Kirmaier, C. Trapping the $P^+B_L^-$ Initial Intermediate State of Charge Separation in Photosynthetic Reaction Centers from *Rhodobacter capsulatus*. *Biochemistry* **2009**, *48*, 2571−2573.
(55) Carter, B.; Boxer, S. G.; Holten, D.; Kirmaier, C. Photochemistry of a Bacterial Photosynthetic Reaction Center Missing the Initial Bacteriochlorophyll Electron Acceptor. *J. Phys. Chem. B* **2012**, *116*, 9971−9982.
(56) Kee, H. L.; Laible, P. D.; Bautista, J. A.; Hanson, D. K.; Holten, D.; Kirmaier, C. Determination of the Rate and Yield of B-Side Quinone Reduction in Rhodobacter Capsulatus Reaction Centers. *Biochemistry* **2006**, *45*, 7314−7322.
(57) Faries, K. M.; Kressel, L. L.; Wander, M. J.; Holten, D.; Laible, P. D.; Kirmaier, C.; Hanson, D. K. High Throughput Engineering to Revitalize a Vestigial Electron Transfer Pathway in Bacterial Photosynthetic Reaction Centers. *J. Biol. Chem.* **2012**, *287*, 8507−8514.
(58) Harris, M. A.; Luehr, C. A.; Faries, K. M.; Wander, M.; Kressel, L.; Holten, D.; Hanson, D. K.; Laible, P. D.; Kirmaier, C. Protein Influence on Charge-Asymmetry of the Primary Donor in Photosynthetic Bacterial Reaction Centers Containing a Heterodimer: Effects on Photophysical Properties and Electron Transfer. *J. Phys. Chem. B* **2013**, *117*, 4028−4041.
(59) Kirmaier, C.; Holten, D. Low-Temperature Studies of Electron Transfer to the M Side of YFH Reaction Centers from Rhodobacter capsulatus. *J. Phys. Chem. B* **2009**, *113*, 1132−1142.
(60) Kirmaier, C.; Laible, P. D.; Hanson, D. K.; Holten, D. B-side Charge Separation in Bacterial Photosynthetic Reaction Centers: Nanosecond-Timescale Electron Transfer from H_B^- to Q_B. *Biochemistry* **2003**, *42*, 2016−2024.
(61) Laible, P. D.; Kirmaier, C.; Udawatte, C. S. M.; Hofman, S. J.; Holten, D.; Hanson, D. K. Quinone Reduction via Secondary B-branch Electron Transfer in Mutant Bacterial Reaction Centers. *Biochemistry* **2003**, *42*, 1718−1730.
(62) Yakovlev, A. G.; Shkuropatova, T. A.; Vasilieva, L. G.; Shkuropatov, A. Y.; Gast, P.; Shuvalov, V. A. Vibrational Coherence in Bacterial Reaction Centers with Genetically Modified B-Branch Pigment Composition. *Biochim. Biophys. Acta* **2006**, *1757*, 369−379.
(63) Zinth, W.; Wachtveitl, J. The First Picoseconds in Bacterial Photosynthesis: Ultrafast Electron Transfer for the Efficient Conversion of Light Energy. *ChemPhysChem* **2005**, *6*, 871−880.
(64) Wang, H. Y.; Lin, S.; Allen, J. P.; Williams, J. C.; Blankert, S.; Laser, C.; Woodbury, N. W. Protein Dynamics Control the Kinetics of Initial Electron Transfer in Photosynthesis. *Science* **2007**, *316*, 747−750.
(65) Kakitani, Y.; Hou, A.; Miyasako, Y.; Koyama, Y.; Nagae, H. Rates of the Initial Two Steps of Electron Transfer in Reaction Centers from Rhodobacter sphaeroides as Determined by Singular-Value Decomposition Followed by Global Fitting. *Chem. Phys. Lett.* **2010**, *492*, 142−149.
(66) Zhu, J. Y.; van Stokkum, I. H. M.; Paparelli, L.; Jones, M. R.; Groot, M. L. Early Bacteriopheophytin Reduction in Charge Separation in Reaction Centers of Rhodobacter sphaeroides. *Biophys. J.* **2013**, *104*, 2493−2502.
(67) Vos, M. H.; Rischel, C.; Jones, M. R.; Martin, J. L. Electrochromic Detection of a Coherent Component in the Formation of the Charge Pair P+HL- in Bacterial Reaction Centers. *Biochemistry* **2000**, *39*, 8353−8361.
(68) Foloppe, N.; Ferrand, M.; Breton, J.; Smith, J. C. Structural Model of the Photosynthetic Reaction-Center of Rhodobacter-Capsulatus. *Proteins: Struct., Funct., Genet.* **1995**, *22*, 226−244.
(69) Laemmli, U. K. Cleavage of Structural Proteins during Assembly of Head of Bacteriophage-T4. *Nature* **1970**, *227*, 680−685.
(70) van der Rest, M.; Gingras, G. Pigment Complement of Photosynthetic Reaction Center Isolated from Rhodospirillum-Rubrum. *J. Biol. Chem.* **1974**, *249*, 6446−6453.
(71) Kirmaier, C.; Laible, P. D.; Czarnecki, K.; Hata, A. N.; Hanson, D. K.; Bocian, D. F.; Holten, D. Comparison of M-side Electron

Transfer in *Rb. sphaeroides* and *Rb. capsulatus* Reaction Centers. *J. Phys. Chem. B* **2002**, *106*, 1799−1808.
(72) Raap, J.; Winkel, C.; Dewit, A. H. M.; Vanhouten, A. H. H.; Hoff, A. J.; Lugtenburg, J. Mass-Spectrometric Determination of Isotopically Labeled Tyrosines and Tryptophans in Photosynthetic Reaction Centers of Rhodobacter-Sphaeroides R-26. *Anal. Biochem.* **1990**, *191*, 9−15.
(73) Arakawa, T.; Shimono, K.; Yamaguchi, S.; Tuzi, S.; Sudo, Y.; Kamo, N.; Saito, H. Dynamic Structure of Pharaonis Phoborhodopsin (Sensory Rhodopsin Ii) And Complex with a Cognate Truncated Transducer As Revealed by Site-Directed C-13 Solid-State NMR. *FEBS Lett.* **2003**, *536*, 237−240.
(74) Barshop, B. A.; Wrenn, R. F.; Frieden, C. Analysis of Numerical-Methods for Computer-Simulation of Kinetic Processes, Development of Kinsim, a Flexible, Portable System. *Anal. Biochem.* **1983**, *130*, 134−145.
(75) O'Reilly, J. E. Oxidation-Reduction Potential of the Ferro-Ferricyanide System in Buffer Solutions. *Biochim. Biophys. Acta* **1973**, *292*, 509−515.
(76) Leach, F.; Armstrong, G. A.; Hearst, J. E. Photosynthetic Genes in Rhodobacter-Capsulatus Can Be Regulated by Oxygen during Dark Respiratory Growth with Dimethylsulfoxide. *J. Gen. Microbiol.* **1991**, *137*, 1551−1556.
(77) Lang, F. S.; Oesterhelt, D. Microaerophilic Growth and Induction of the Photosynthetic Reaction Center in Rhodopseudomonas-Viridis. *J. Bacteriol.* **1989**, *171*, 2827−2834.
(78) Chuang, J. I. Understanding Unidirectional Electron Transfer in the Photosynthetic Reaction Center using Protein Engineering. PhD Thesis, Stanford University, 2007.
(79) Sigala, P. A.; Fafarman, A. T.; Schwans, J. P.; Fried, S. D.; Fenn, T. D.; Caaveiro, J. M. M.; Pybus, B.; Ringe, D.; Petsko, G. A.; Boxer, S. G.; Herschlag, D. Quantitative Dissection of Hydrogen Bond-Mediated Proton Transfer in the Ketosteroid Isomerase Active Site. *Proc. Natl. Acad. Sci. U.S.A.* **2013**, *110*, E2552−E2561.
(80) Mcdermott, A. E.; Thompson, L. K.; Winkel, C.; Farrar, M. R.; Pelletier, S.; Lugtenburg, J.; Herzfeld, J.; Griffin, R. G. Mechanism of Proton Pumping in Bacteriorhodopsin by Solid-State NMR: The Protonation State of Tyrosine in the Light-Adapted and M-States. *Biochemistry* **1991**, *30*, 8366−8371.
(81) Takeda, M.; Jee, J.; Ono, A. M.; Terauchi, T.; Kainosho, M. Hydrogen Exchange Rate of Tyrosine Hydroxyl Groups in Proteins As Studied by the Deuterium Isotope Effect on C-zeta Chemical Shifts. *J. Am. Chem. Soc.* **2009**, *131*, 18556−18562.
(82) Fufina, T. Y.; Vasilieva, L. G.; Khatypov, R. A.; Shkuropatov, A. Y.; Shuvalov, V. A. Substitution of Isoleucine L177 by Histidine in Rhodobacter sphaeroides Reaction Center Results in the Covalent Binding of P-A Bacteriochlorophyll to the L Subunit. *FEBS Lett.* **2007**, *581*, 5769−5773.
(83) Potter, J. A.; Fyfe, P. K.; Frolov, D.; Wakeham, M. C.; van Grondelle, R.; Robert, B.; Jones, M. R. Strong Effects of an Individual Water Molecule on the Rate of Light-Driven Charge Separation in the Rhodobacter sphaeroides Reaction Center. *J. Biol. Chem.* **2005**, *280*, 27155−27164.
(84) Kirmaier, C.; Weems, D.; Holten, D. M-side Electron Transfer in Reaction Center Mutants with a Lysine near the Nonphotoactive B Bacteriochlorophyll. *Biochemistry* **1999**, *38*, 11516−11530.
(85) Kirmaier, C.; Gaul, D.; DeBey, R.; Holten, D.; Schenck, C. C. Charge Separation in a Reaction Center Incorporating Bacteriochlorophyll in Place of Photoactive Bacteriopheophytin. *Science* **1991**, *251*, 922−927.
(86) Breton, J.; Martin, J. L.; Lambry, J. C.; Robles, S. J.; Youvan, D. C. Ground State and Femtosecond Transient Absorption Spectroscopy of a Mutant of *Rhodobacter capsulatus* which Lacks the Initial Electron Acceptor Bacteriopheophyrin. In *Structure and Function of Bacterial Photosynthetic Reaction Centers*; Michel-Beyerle, M. E., Ed.; Springer-Verlag: New York, 1990; pp 293−302.
(87) Robles, S. J.; Breton, J.; Youvan, D. C. Partial Symmetrization of the Photosynthetic Reaction Center. *Science (Washington, D.C.)* **1990**, *248*, 1402−1405.
(88) Kirmaier, C.; Holten, D. Evidence that a Distribution of Bacterial Reaction Centers Underlies the Temperature- and Detection-Wavelength-Dependence of the Rates of the Primary Electron Transfer Reactions. *Proc. Natl. Acad. Sci. U.S.A.* **1990**, *97*, 3522−3556.
(89) Wang, H. Y.; Lin, S.; Katilius, E.; Laser, C.; Allen, J. P.; Williams, J. C.; Woodbury, N. W. Unusual Temperature Dependence of Photosynthetic Electron Transfer due to Protein Dynamics. *J. Phys. Chem. B* **2009**, *113*, 818−824.
(90) Fyfe, P. K.; Ridge, J. R.; McAuley, K. E.; Cogdell, R. J.; Isaacs, N. W.; Jones, M. R. Structural Consequences of the Replacement of Glucine M203 with Aspartic Acid in the Reaction Center from *Rhodobacter sphaeroides*. *Biochemistry* **2000**, *39*, 5953−5960.
(91) Yakovlev, A. G.; Jones, M. R.; Potter, J. A.; Fyfe, P. K.; Vasilieva, L. G.; Shkuropatov, A. Y.; Shuvalov, V. A. Primary Charge Separation between P* and BA: Electron-Transfer Pathways in Native and Mutant GM203L Bacterial Reaction Centers. *Chem. Phys.* **2005**, *319*, 297−307.
(92) Yakovlev, A. G.; Khmelnitsky, A. Y.; Shuvalov, V. A. Femtosecond Charge Separation in Dry Films of Reaction Centers of Rhodobacter sphaeroides and Chloroflexus aurantiacus. *Biochemistry (Moscow)* **2012**, *77*, 444−455.
(93) Ivashin, N.; Larsson, S. Trapped Water Molecule in the Charge Separation of a Bacterial Reaction Center. *J. Phys. Chem. B* **2008**, *112*, 12124−12133.
(94) Ivashin, N. V.; Shchupak, E. E. Mechanism by Which a Single Water Molecule Affects Primary Charge Separation Kinetics in a Bacterial Photosynthetic Reaction Center of Rhodobacter sphaeroides. *Opt. Spectrosc.* **2012**, *113*, 474−486.